PERGAMON

International Journal of Heat and Mass Transfer 42 (1999) 2015–2029

International Journal of HEAT and MASS TRANSFER

Gravitational and centrifugal buoyancy effects in curved square channels with conjugated boundary conditions

T.W. Gyves[a,*], T.F. Irvine, Jr.[b], M.H.N. Naraghi[c]

[a] *Department of Engineering, State University of New York Maritime College, Throggs Neck, NY 10465, U.S.A.*
[b] *Department of Mechanical Engineering, State University of New York at Stony Brook, Stony Brook, NY 11794, U.S.A.*
[c] *Department of Mechanical Engineering, Manhattan College, Riverdale, NY 10471, U.S.A.*

Received 14 November 1997; in final form 25 August 1998

Abstract

Fully developed laminar flow in a curved square channel with peripheral wall conduction is examined. The wall average Nusselt number, $\overline{Nu}$, is presented as a function of four parameters: the wall conduction parameter, ϕ, the Prandtl number, and two Grashof numbers, Gr_g and Gr_c, which represent the gravitational and centrifugal forces, respectively, present in a variable density fluid. Numerical solutions are presented for $4.4 < De < 210.9$, $0.01 < \phi < 20.0$, and $0.01 < Pr < 7.2$. For constant De, curved channel mixed convection $\overline{Nu}$ values are demonstrated to be reduced below the curved channel forced convection values due to a weakening of the secondary flow field. A curve illustrating the relationship between ϕ_{eff}, defined as the value of ϕ at which a constant wall temperature boundary condition can be assumed, and De is presented.

Nomenclature

a width or height of a curved square channel
C_p specific heat
dp^+/dz^+ dimensionless axial pressure gradient
De Dean number, $=Re(D_h/R)^{1/2}$
D_h hydraulic diameter
f friction factor
g gravitational acceleration
Gr' gravitational Grashof number as defined in [16, 18–20]
Gr_c centrifugal Grashof number, $=\beta\bar{W}^2 D_h^4 q''/Rv^2 k_f$
Gr_g gravitational Grashof number, $=\beta g D_h^4 q''/v^2 k_f$
$\bar{h}$ average heat transfer coefficient
$H1$ constant peripheral wall temperature boundary condition
$H2$ constant peripheral heat flux boundary condition
I, J X and Y nodal points on numerical calculation grid
k thermal conductivity
n^+ dimensionless normal coordinate
$\overline{Nu}$ Nusselt number, $=\bar{h}D_h/k_f$, $=1/(\overline{T_w^+}-T_b^+)$
p^+ dimensionless pressure, $=P/(\rho v^2/D_h^2)$
P pressure
Pe Peclet number, $=\overline{W}D_h/\alpha_f$
Pr Prandtl number, $=v/\alpha$
q'' heat transferred per unit surface area of channel wall
q''' internal heat generation per unit volume
r^+ dimensionless radius of curvature, $=R/D_h$
R radius of curvature of a curved square channel
Ra Rayleigh number, $=Gr_g Pr$
Ra' Rayleigh number as defined in [22]
Re Reynolds number, $=\overline{W}D_h/v_f$, $=\overline{w^+}$
S source term
t duct wall thickness
T temperature
T^+ dimensionless temperature, $=(T-T_0)/(q''D_h/k_f)$
u^+, v^+, w^+ dimensionless velocity components, $=(U, V, W)D_h/v$
U, V, W velocity components in the X-, Y-, and Z-directions
$\overline{w^+}$ average dimensionless axial velocity
$\overline{W}$ average axial velocity
x^+, y^+, z^+ dimensionless coordinates, $=(X, Y, Z)/D_h$
X, Y, Z Cartesian coordinates.

Greek symbols
α thermal diffusivity

* Corresponding author. Tel: 001 516 868 7729

0017–9310/99/$ - see front matter
PII: S0017–9310(98)00293–2

β coefficient of volumetric expansion
Γ diffusion coefficient in the SIMPLE algorithm
ε convergence criterion used in the numerical procedure
μ dynamic viscosity
v kinematic viscosity
ρ density
σ dependent variable in the SIMPLE algorithm
ϕ dimensionless wall conduction parameter, $=k_w t/k_f D_h$.

Subscripts
b bulk
eff value at which $\overline{Nu} = 0.99\overline{Nu}_{H1}$
f fluid
i, j nodal points on numerical grid
l local value
s value for a straight channel
T total
w wall
0 reference value, or forced convection value
∞ reference value
σ value corresponding to a particular dependent variable.

1. Introduction

With engineering applications as diverse as compact heat exchangers and turbine blade and rocket engine cooling passages, the study of curved channel fluid flow and heat transfer has been accorded widespread attention in recent years. One of the more interesting aspects of curved channel flows is the introduction of a secondary flow pattern in the duct cross-section resulting from the imbalance developed between the centrifugal force and the radial pressure fields. Eustice [1, 2] was the first to demonstrate the existence of this secondary flow pattern by injecting dyes into a curved pipe flow stream. Dean's subsequent analytical studies [3, 4] determined that curved pipe flow could be characterized by a single parameter, the Dean number, *De*. A key assumption in both of Dean's early studies was that the radius of curvature R was significantly larger than a, where a in this case represented the pipe radius, which would at first glance appear to be a rather limiting case. Recent studies (Cheng et al. [5], Thangam and Hur [6], and Gia and Sokhey [7]) on curved rectangular ducts, however, indicate that the curvature effect is completely contained within the Dean number for values of r^+ as low as from 3–10. It appears, therefore, that *De* is the governing parameter in curved channel flow for a much wider range of r^+ values than Dean's original formulation would imply.

The secondary flow pattern which distinguishes curved channel flows presents itself, over an initial range of *De*, as a single pair of counter-rotating vortices placed symmetrically above and below the channel's horizontal centerline. At higher values of *De* an additional pair of counter-rotating vortices appears near the outer wall, a transition known as Dean's Instability. The effect of this enhanced secondary flow, as well as the distortions to the fluid axial velocity profiles occurring in a curved channel, on local and overall channel heat transfer performance has been the central focus of numerous analytical and experimental studies examining curved channels with polar, circular, elliptic and rectangular cross-sections. The vast majority of these studies have assumed that fluid density is constant. Overall heat transfer rates in curved channels have been shown to be significantly increased due to the presence of the secondary flow field. Mori and Nakayama [8] noted a four- to six-fold increase in $\overline{Nu}$ over the value for a straight pipe for *De* ranging from 500–1000. Mori et al. [9] presented both analytical and experimental data for curved square channels subject to intense secondary flows, and hypothesized that the fluid flow and temperature fields could be divided into two regions: a core wherein fluid viscosity and heat conduction are dominated by the inertial effect of the secondary flow, and a boundary layer near the channel wall where viscosity and conduction effects must be considered. The data presented indicated a dramatic increase in $\overline{Nu}$ with increased *De*. In a study of forced convection in curved rectangular channels with aspect ratios ranging between 0.2 and 5.0 by Cheng and Akiyama [10], the authors indicated that changes in either *Pr* or *De* have a significant effect on $\overline{Nu}$, a conclusion reported once again by Zapryanov et al. [11] in their examination of curved tubes. Komiyama et al. [12] examined forced convection in rectangular channels with aspect ratios ranging from 0.8–5.0 and a curvature ratio, r^+, equal to 100.0. Local Nusselt number profiles were presented along the channel's four walls, and the data confirmed that local heat transfer rates were maximized along the outer wall. However, the authors noted that at elevated values of *De*, Nu_l is minimized at the central part of the outer wall due to the appearance of a region of stagnation flow. Data for curved square channels were presented by Hwang and Chao [13], who also included the effect of fluid axial conduction in low *Pe* flows. The authors correlated $\overline{Nu}$ with the product $Pr\,De^2$.

Other studies have analyzed the combined effect of channel curvature and fluid buoyancy. However, the studies which have sought to include the effect of fluid buoyancy have, without exception, neglected the influence of variable density in the transverse or radial direction, thereby limiting their analysis to a study of the influence of gravitational buoyancy forces alone on curved channel flow and heat transfer. In the discussion to follow, only gravitational buoyancy and constant density centrifugal forces are considered by the investigators. Yao and Berger [14] examined both horizontal and vertical curved tubes subject to a uniform axial temperature gradient, and noted the effect of buoyancy forces on the

secondary flow streamlines. In the presence of even a moderate buoyancy force ($Re\,Ra = 1000$), the streamlines were rotated nearly 45° clockwise in the duct cross-section, and the authors noted that at sufficiently high values of this parameter, the dividing streamline separating the counter-rotating vortices appears in the vertical direction rather than in the usual horizontal direction. The authors presented correlations for both horizontal and vertical tube Nusselt numbers as a function of *Pr*, *Re*, *Ra*, and *De*. Prusa and Yao [15] examined curved heated tubes subject to a constant axial temperature gradient, and noted a drastic reduction in the mass flow rate due to the presence of the curvature-induced secondary flow pattern. Secondary flow streamline plots illustrating the interaction of centrifugal forces and buoyancy forces were presented for three values of *Re Ra*, the parameter which measures the strength of the buoyancy forces in the fluid. The authors identified three flow regimes in curved tubes under the influence of buoyancy forces, one corresponding to flows dominated by centrifugal forces, one for buoyancy dominated flows, and the third representing flows in which both forces are significant. These regimes are represented graphically as a function of *De* and *Re Ra*. Lee et al. [16] examined the influence of buoyancy on fully developed laminar flow heat transfer in curved tubes under thermal boundary conditions of axially uniform heat flux and peripherally uniform wall temperature. The results presented clearly indicate that heat transfer rates in curved tubes are enhanced by the effect of gravitational buoyancy, which serves to further increase the intensity of the secondary flow field present in a curved channel. However, the authors noted that the effect of buoyancy on $\overline{Nu}$ decreases as *De* increases and the flow is increasingly dominated by centrifugal forces. Two very interesting regimes can be noted in the data presented. In the first, centrifugal forces are seen to dominate flow regardless of the value of Gr'. This holds for $Gr'/De^2 < 2.5$. Conversely, buoyancy forces are dominant irrespective of the value of *De* for $Gr'/De^2 > 10$. Plots of secondary flow streamlines are skewed towards a vertical line of symmetry when gravitational buoyancy is included. Dong and Ebadian followed their earlier analysis [17] of curved elliptic channel flows with an examination of the effect of a buoyancy-induced secondary flow on the friction factor and $\overline{Nu}$ in curved elliptic ducts [18]. The boundary conditions considered were axially uniform heat flux and peripherally uniform wall temperature. Once again, the buoyancy force was found to disrupt the symmetry of the secondary flow streamlines, with the counter-rotating vortices no longer symmetric about the horizontal axis. With buoyancy forces included, this line of symmetry was disturbed, with the center of the upper and lower vortices shifting toward the outer and inner walls, respectively. The data presented indicate that *De* decreases and the friction factor and $\overline{Nu}$ both increase with increased values of Gr'. Sankar et al. [19] performed a numerical study of mixed convection in curved square channels with thermal boundary conditions of peripherally uniform wall temperature and axially uniform heat flux. Forced and mixed convection results for both the friction factor ratio $f\,Re/f\,Re_s$ and Nusselt number ratio $\overline{Nu}/\overline{Nu}_s$ are provided for $Pr = 0.73$ over a wide range of *De* and Gr' values. The authors noted that the effect of gravitational buoyancy forces is to increase the secondary flow and thus increase both the flow resistance and heat transfer rate. Goering et al. [20] have recently analyzed the influence of gravitational buoyancy in fully developed curved tube flow for both the uniform peripheral wall temperature (*H*1) and uniform peripheral wall heat flux (*H*2) thermal boundary conditions. It is important to note that their study is the first known analysis of the *H*2 boundary condition in curved tube buoyant flow. Each of the curved channel buoyancy studies cited above employed the *H*1 boundary condition, and the results presented by Goering et al. for the boundary condition are in agreement with these earlier studies, indicating that the effect of buoyancy was to increase both the friction factor and the Nusselt number relative to the forced convection case. Data presented for the constant peripheral wall heat flux boundary condition indicated that the effect of buoyancy was to reduce both the friction factor and the Nusselt number relative to the forced convection case. The authors attribute this surprising result to a reduction in secondary flow field intensity resulting from a stratification of the fluid temperature field which is caused by the peripheral wall temperature variation associated with the *H*2 boundary condition. This weakening of the secondary flow field, and the resulting reduction in $\overline{Nu}$ below its forced convection value, will be shown in the present study to occur in curved square channels for both the *H*1 and *H*2 boundary conditions.

The curved channel studies published to date have all been limited by their adoption of the idealized *H*1 or *H*2 thermal boundary conditions. These boundary conditions are typically employed in order to simplify the analytical model, but they hide one of the more interesting aspects of the problem at hand, namely, the peripheral conduction which occurs in the channel wall itself. One must assume that the channel wall material has an infinitely high value of thermal conductivity in order for the *H*1 condition to accurately model the system. Conversely, the *H*2 boundary condition requires that the channel wall have a zero thermal conductivity, in which case all heat generated within the wall in a specific control volume is transferred directly to the fluid at that same location without any peripheral conduction. Eckert and Irvine [21] noted that a wall conduction parameter, ϕ, could be employed to characterize the conjugated nature of the channel flow problem, and the present analysis provides $\overline{Nu}$ solutions for a complete range of values of this parameter, including the idealized asymptotic solutions $\overline{Nu}_{H1}$ and $\overline{Nu}_{H2}$.

2. Analysis

The curved square channel is illustrated in Fig. 1. Flow is assumed to be laminar, fully developed and steady, and fluid density variations with temperature are modeled using the Boussinesq approximation. All other physical properties are assumed constant. It is further assumed that the radius of curvature, R, is large compared to the channel dimension a. As such, the model neglects all terms of the order $1/R$ and $1/R^2$, with the exception of the centrifugal force term. The exterior channel surface is adiabatic, and the rate of internal heat generation is uniform throughout the channel walls, which are assumed to be sufficiently thin such that channel wall conduction can be modeled as one-dimensional along the channel perimeter. The governing equations can be written as follows [10, 12]:

Continuity equation

$$\frac{\partial U}{\partial X}+\frac{\partial V}{\partial Y}=0. \tag{1}$$

Momentum equations

$$\rho\left[U\frac{\partial U}{\partial X}+V\frac{\partial U}{\partial Y}\right]=-\frac{\partial P}{\partial X}+\rho\frac{W^2}{R}+\mu\left[\frac{\partial^2 U}{\partial X^2}+\frac{\partial^2 U}{\partial Y^2}\right] \tag{2}$$

$$\rho\left[U\frac{\partial V}{\partial X}+V\frac{\partial V}{\partial Y}\right]=-\frac{\partial P}{\partial Y}-\rho g+\mu\left[\frac{\partial^2 V}{\partial X^2}+\frac{\partial^2 V}{\partial Y^2}\right] \tag{3}$$

$$\rho\left[U\frac{\partial W}{\partial X}+V\frac{\partial W}{\partial Y}\right]=-\frac{\partial P}{\partial Z}+\mu\left[\frac{\partial^2 W}{\partial X^2}+\frac{\partial^2 W}{\partial Y^2}\right]. \tag{4}$$

Fluid energy equation

$$\rho C_{\mathrm{p}}\left[U\frac{\partial T}{\partial X}+V\frac{\partial T}{\partial Y}+W\frac{\partial T}{\partial Z}\right]=k\left[\frac{\partial^2 T}{\partial X^2}+\frac{\partial^2 T}{\partial Y^2}\right]. \tag{5}$$

The present analysis also assumes that the curved channel flow can be modeled as a parabolic flow field, which results in a significant degree of simplification in the governing equations. The dominant flow direction in curved channels is axial, and the flow can be categorized as parabolic in that direction. Convection will dominate diffusion in this direction and hence, the axial diffusion terms which appear in the Navier–Stokes equations can be ignored. The fluid pressure field is assumed to be 'decoupled' in parabolic flows, with the total fluid pressure at any point, P_{T}, considered to be the sum of a cross-stream average pressure, $P_0(Z)$, which is a function of the streamwise coordinate alone, and a pressure $P(X, Y)$ which varies in the cross-stream direction. That is

$$P_{\mathrm{T}}=P_0(Z)+P(X, Y) \tag{6}$$

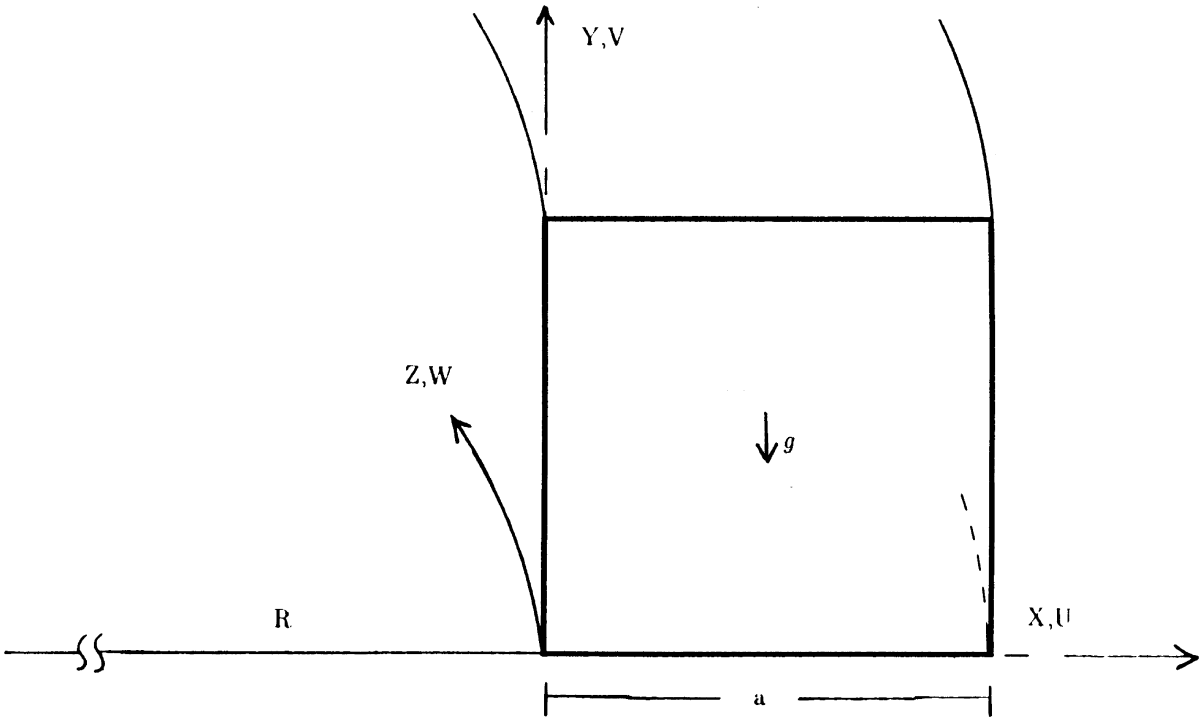

Fig. 1. Curved channel coordinate system.

with the pressure field in the transverse direction, $P(X, Y)$, represented as follows (see [18, 22–24]):

$$P(X, Y) = P'(X, Y) - \rho_\infty g Y + \rho_\infty \frac{W^2}{R} X. \tag{7}$$

For fully developed flow, the axial pressure gradient, $\partial P_0/\partial Z$, is constant. Noting that $(\partial P_T/\partial X) = (\partial P/\partial X)$ and $(\partial P_T/\partial Y) = (\partial P/\partial Y)$, we can then write the following expressions for the transverse pressure gradients:

$$\frac{\partial P_T}{\partial X} = \frac{\partial P'}{\partial X} + \frac{\rho_\infty W^2}{R} + \frac{2\rho_\infty WX}{R}\frac{\partial W}{\partial X} \tag{8}$$

and

$$\frac{\partial P_T}{\partial Y} = \frac{\partial P'}{\partial Y} - \rho_\infty g + \frac{2\rho_\infty WX}{R}\frac{\partial W}{\partial Y}. \tag{9}$$

The last terms in equations (8) and (9) are neglected in the present analysis, since both are of order $1/R$. This simplification is utilized in the development of the governing equations (1)–(5) and is valid only in the case of large channel radius of curvature.

Rearranging the body force terms in the X- and Y-momentum equations, the governing equations for the present system can be written in the following form (in the equations below, P' is noted simply as P for clarity):

Continuity equation

$$\frac{\partial U}{\partial X} + \frac{\partial V}{\partial Y} = 0. \tag{10}$$

Momentum equations:

$$\rho\left[U\frac{\partial U}{\partial X} + V\frac{\partial U}{\partial Y}\right] = -\frac{\partial P}{\partial X} + [\rho - \rho_\infty]\frac{W^2}{R} + \mu\left[\frac{\partial^2 U}{\partial X^2} + \frac{\partial^2 U}{\partial Y^2}\right] \tag{11}$$

$$\rho\left[U\frac{\partial V}{\partial X} + V\frac{\partial V}{\partial Y}\right] = -\frac{\partial P}{\partial Y} + [\rho_\infty - \rho]g + \mu\left[\frac{\partial^2 V}{\partial X^2} + \frac{\partial^2 V}{\partial Y^2}\right] \tag{12}$$

$$\rho\left[U\frac{\partial W}{\partial X} + V\frac{\partial W}{\partial Y}\right] = -\frac{\partial P}{\partial Z} + \mu\left[\frac{\partial^2 W}{\partial X^2} + \frac{\partial^2 W}{\partial Y^2}\right]. \tag{13}$$

Fluid energy equation

$$\rho C_p\left[U\frac{\partial T}{\partial X} + V\frac{\partial T}{\partial Y} + W\frac{\partial T}{\partial Z}\right] = k\left[\frac{\partial^2 T}{\partial X^2} + \frac{\partial^2 T}{\partial Y^2}\right]. \tag{14}$$

The buoyancy terms which appear in the X- and Y-momentum equations above can be rewritten in terms of the Boussinesq approximation. We can then express the body force terms which appear in these two equations in the following manner:

$$[\rho - \rho_\infty]\frac{W^2}{R} = -\rho_\infty \beta (T - T_\infty)\frac{W^2}{R} \tag{15}$$

and

$$[\rho_\infty - \rho]g = \rho_\infty \beta (T - T_\infty) g. \tag{16}$$

Substitution of the dimensionless variables listed in the nomenclature leads to the following set of dimensionless equations:

$$\frac{\partial u^+}{\partial x^+} + \frac{\partial v^+}{\partial y^+} = 0 \tag{17}$$

$$u^+\frac{\partial u^+}{\partial x^+} + v^+\frac{\partial u^+}{\partial y^+} = -\frac{\partial p^+}{\partial x^+} - Gr_c T^+ + \frac{\partial^2 u^+}{\partial x^{+2}} + \frac{\partial^2 u^+}{\partial y^{+2}} \tag{18}$$

$$u^+\frac{\partial v^+}{\partial x^+} + v^+\frac{\partial v^+}{\partial y^+} = -\frac{\partial p^+}{\partial y^+} + Gr_g T^+ + \frac{\partial^2 v^+}{\partial x^{+2}} + \frac{\partial^2 v^+}{\partial y^{+2}} \tag{19}$$

$$u^+\frac{\partial w^+}{\partial x^+} + v^+\frac{\partial w^+}{\partial y^+} = -\frac{\partial p^+}{\partial z^+} + \frac{\partial^2 w^+}{\partial x^{+2}} + \frac{\partial^2 w^+}{\partial y^{+2}} \tag{20}$$

$$u^+\frac{\partial T^+}{\partial x^+} + v^+\frac{\partial T^+}{\partial y^+} + w^+\frac{\partial T^+}{\partial z^+} = \frac{1}{Pr}\left[\frac{\partial^2 T^+}{\partial x^{+2}} + \frac{\partial^2 T^+}{\partial y^{+2}}\right]. \tag{21}$$

The equations are subject to the following boundary conditions:

At the channel wall

$$u^+ = v^+ = w^+ = 0. \tag{22}$$

The energy equations for the channel walls are derived by balancing the net conduction across a typical control volume with the rate of internal heat generation and the convection heat transfer between the wall and fluid. For example, the left wall equation may be written as:

$$k_w t(1)\frac{d^2 T_w}{dY^2} dY + q''' t\, dY(1) = -k_f\, dY(1)\left(\frac{dT}{dX}\right)_{w\text{–}f}. \tag{23}$$

Employing the definitions for the dimensionless temperature and the wall conduction parameter, ϕ, the left wall energy equation becomes

$$\phi\frac{d^2 T_w^+}{dy^{+2}} + 1 + \left(\frac{dT^+}{dx^+}\right)_{w\text{–}f} = 0. \tag{24}$$

The equations for the remaining walls can be easily derived in a similar manner.

The appearance of the parameter ϕ in the wall energy equations is a direct consequence of the conjugated nature of this system. Eckert and Irvine [21] were the first to identify this important parameter in a study of convective heat transfer in triangular ducts. It is helpful at this point to examine its physical interpretation, since it plays a significant role in the analysis to follow. We have defined ϕ as

$$\phi = \frac{k_w t}{k_f D_h} \tag{25}$$

and as can be readily seen, infinitely large or small values

of this parameter describe two distinct thermal boundary conditions. In the first of these (i.e. $\phi \to \infty$), the channel wall is termed 'thermally thick', with k_w and/or t assuming asymptotically large values. In this case one would expect that the channel wall would act as a strong agent for conducting the heat generated in any section to neighboring areas. The result would therefore be a channel with nearly uniform wall temperatures along the entire perimeter, a situation very similar to that predicted by the $H1$ boundary condition. For asymptotically low values of ϕ (i.e., $\phi \to 0$), the channel wall is termed 'thermally thin'. A number of factors can contribute to such a condition, including extremely low values of k_w and t, or very large values of k_f. Poor wall conductivity, coupled with a minimal path of resistance (i.e., small t) between the wall and the fluid would result in the energy generated within the wall at any point being transferred to the fluid at that same location through convection, rather than being conducted along the wall perimeter as described in the first case above. Since the assumption is made that the internal heat generation is uniform around the perimeter, this would result in a constant wall-to-fluid heat flux around the channel perimeter, commonly referred to as the $H2$ boundary condition.

3. Numerical solution

Patankar [25] notes that the basic equation governing all analytical models of heat and mass transfer and fluid flow is a conservation equation which includes both convection and diffusion terms, as well as an appropriate source term. This general equation can be written as follows:

$$\nabla\cdot(\rho\bar{U}\sigma) = \nabla\cdot(\Gamma_\sigma\nabla\sigma) + S_\sigma. \tag{26}$$

Here, $\bar{U}$ is the three-dimensional velocity vector with X, Y, and Z components, and Γ and S are the diffusion coefficient and source term, respectively, corresponding to a particular dependent variable σ. The dependent variable σ can represent dimensional or dimensionless quantities, such as a velocity component (U or u^+, as in the case of the x^+-momentum equation), or the fluid temperature (T or T^+, as in the case of the fluid energy equation). This generalized conservation equation can be written in terms of dimensionless variables, with σ representing a dimensionless dependent variable, and Γ and S the appropriate diffusion coefficient and source term, respectively. In Cartesian-tensor form, the (steady state) dimensionless conservation equation can be written as follows:

$$\frac{\partial}{\partial x_i}(u_i\sigma) = \frac{\partial}{\partial x_i}\left(\Gamma_\sigma\frac{\partial\sigma}{\partial x_i}\right) + S_\sigma. \tag{27}$$

In the case of the dimensionless x-momentum equation, we have the following:

$$\sigma = u^+ \tag{28}$$

and

$$\Gamma_\sigma = 1. \tag{29}$$

The expressions for the dependent variable, σ, the diffusion coefficient, Γ_σ, and the appropriate source term, S_σ for each of the dimensionless equations are defined in Table 1.

The solution procedure employed in the present study is based upon the algorithm outlined in Patankar, working in conjunction with a new subroutine to account for the thermal boundary condition of peripheral wall conduction and wall-to-fluid convection. For given values of r^+, $\mathrm{d}p^+/\mathrm{d}z^+$, Pr, Gr_g, Gr_c, and ϕ, the numerical solution procedure starts with an initial guess for u^+, v^+, w^+, T^+, and p^+ at each nodal location. Updated values for all dependent parameters are then obtained using the SIMPLE algorithm, with the convective and diffusive terms formulated using a power-law scheme. The wall energy subroutine provides updated wall temperature data at each iteration. This iterative procedure is then repeated until the following convergence criterion is satisfied at each node:

$$\frac{\sigma_{i,j}^{k+1} - \sigma_{i,j}^{k}}{\sigma_{i,j}^{k+1}} < \varepsilon_\sigma \tag{30}$$

where σ represents u^+, v^+, w^+, and T^+, the subscripts i, j refer to nodes on the numerical grid, and $k+1$ refers to the latest iteration. The following values for the convergence criterion, ε, were selected and used throughout the analysis:

$$\varepsilon_{u^+,v^+} = 10^{-3} \tag{31}$$

$$\varepsilon_{w^+,T^+} = 10^{-4}. \tag{32}$$

These convergence parameter values are similar to those utilized by Komiyama et al. and Cheng et al. ($\varepsilon = 10^{-3}$) and Dong and Ebadian ($\varepsilon = 10^{-4}$). A range of underrelaxation factors was employed during the calculation procedures to assist in obtaining a convergent solution. Values ranging from 0.25 to 0.5 were used depending upon the magnitude of Gr_g and Gr_c, with the smaller relaxation factors utilized at higher values of Gr_g and Gr_c.

The numerical results of primary interest in the present study are the calculated values for the Dean number (De),

Table 1
Dimensionless conservation equation variables

σ	Γ_σ	S_σ
u	1	$S_u = -Gr_c\,T$
v	1	$S_v = +Gr_g\,T$
w	1	$S_w = -(\mathrm{d}p/\mathrm{d}z)$
T	$1/Pr$	$S_T = -4(w/Re\,Pr)$

friction factor (f) and the average Nusselt number ($\overline{Nu}$). The Dean number is defined as

$$De = \frac{Re}{r^{+0.5}}. \tag{33}$$

The Reynolds number, Re, which appears in this equation is based upon the cross-sectional averaged axial velocity $\overline{W}$, calculated by integrating over the channel cross-section:

$$\overline{W} = \frac{\int W \,\mathrm{d}x\,\mathrm{d}y}{\int \mathrm{d}x\,\mathrm{d}y}. \tag{34}$$

The friction factor based upon the channel hydraulic diameter, f_{D_h}, is given by

$$f_{D_h} = \frac{-2(\mathrm{d}P/\mathrm{d}Z)D_h}{\rho \overline{W}^2}. \tag{35}$$

Applying the definitions for the dimensionless variables p^+ and z^+, it can be easily shown that the product of the friction factor and Reynolds number reduces to the following simplified expression

$$f\,Re = -2\frac{\mathrm{d}p^+/\mathrm{d}z^+}{\overline{w^+}}. \tag{36}$$

The average wall-to-fluid heat transfer coefficient, $\bar{h}$, is defined as follows:

$$\bar{h} = \frac{q''}{\overline{T_w} - T_b} \tag{37}$$

where q'' represents the heat flux between the channel wall and the fluid, $\bar{T}_w$ is the average wall temperature around the channel perimeter, and T_b is the fluid bulk temperature. The average Nusselt number, $\overline{Nu}$, can be expressed as

$$\overline{Nu} = \frac{1}{\overline{T_w^+} - T_b^+}. \tag{38}$$

In the present analysis, $\overline{T_w^+}$ is the arithmetic average of the calculated wall temperatures at each wall node around the channel perimeter, i.e.,

$$\overline{T_w^+} = \frac{1}{n}\sum_{i=1}^{n} T_i^+ \tag{39}$$

where n represents the number of wall nodes and T_i^+ is the temperature at wall node i. The dimensionless fluid bulk temperature, T_b^+, is calculated in a manner similar to that outlined for $\overline{W}$ above, i.e.

$$T_b^+ = \frac{\int T^+ w^+ \,\mathrm{d}x^+\,\mathrm{d}y^+}{\int w^+ \,\mathrm{d}x^+\,\mathrm{d}y^+}. \tag{40}$$

Numerical results for the curved channel flow field and $\overline{Nu}$ have been obtained using 30×30 and 40×40 numerical grids, with the latter employed at higher values of De. This grid resolution is comparable to that employed by Cheng and Akiyama (32×32) and Komiyama et al. and Cheng et al. (20×20) in their analyses of curved square channels. Curved channel data were obtained using a curvature ratio of $r^+ = 100$. In addition, several straight channel solutions are presented for the asymptotic case of an infinite radius of curvature (i.e., $r^+ \to \infty$). For the purposes of the present study, a straight channel is modeled using a radius of curvature of $r^+ = 1000$.

4. Results and discussion

4.1. Straight square channels

4.1.1. Forced convection flow field ($\mathrm{Gr}_g = 0$)

The numerical solution yielded a value for the product of the friction factor and Re of $f\,Re = 14.163$, which is in good agreement with the value of 14.227 presented in Shah and London [26].

4.1.2. Mixed convection flow field ($\mathrm{Gr}_g \neq 0$)

The effect of gravitational buoyancy in a straight channel with constant peripheral wall temperature was analyzed by setting $\phi = 20$, and the results are illustrated in Fig. 2(a), where streamlines are presented for the case of $Gr_g = 25\,000$ and $Pr = 0.73$. The following expression (see Gyves [27]) is utilized to relate the data obtained in the present study with that presented by Cheng and Hwang [22]:

$$Re\,Ra' = 4Gr_g. \tag{41}$$

In order to compare the results presented in this earlier study for the case of $Re\,Ra' = 1.03E+5$, the value of Gr_g in the present analysis was set at 25 000. Figure 2(a) is in excellent agreement with the results presented by Cheng and Hwang. The gravitational buoyancy forces produce a pair of counter-rotating vortices which are symmetric about the vertical centerline of the channel ($x^+ = 0.5$), and the streamline magnitudes closely approximate those presented earlier. It is interesting to note that the center of circulation is shifted below the horizontal line $y^+ = 0.5$, indicating that the strongest secondary flow occurs in the lower half of the channel cross-section.

The effect of buoyancy forces on the straight channel friction factor is demonstrated in Fig. 2(b), where results for fRe/fRe_0 (the subscript indicating the forced convection value) are presented and compared once again to data previously reported by Cheng and Hwang for the constant peripheral wall temperature boundary condition and $Pr = 0.73$. The data offer strong evidence that the secondary flow pattern which is produced by the buoyancy forces results in an increase in friction resistance above that found in straight channel forced convection.

4.1.3. Conjugated forced convection heat transfer ($\mathrm{Gr}_g = 0$)

The numerical solution for conjugated forced convection heat transfer in a straight square channel is illus-

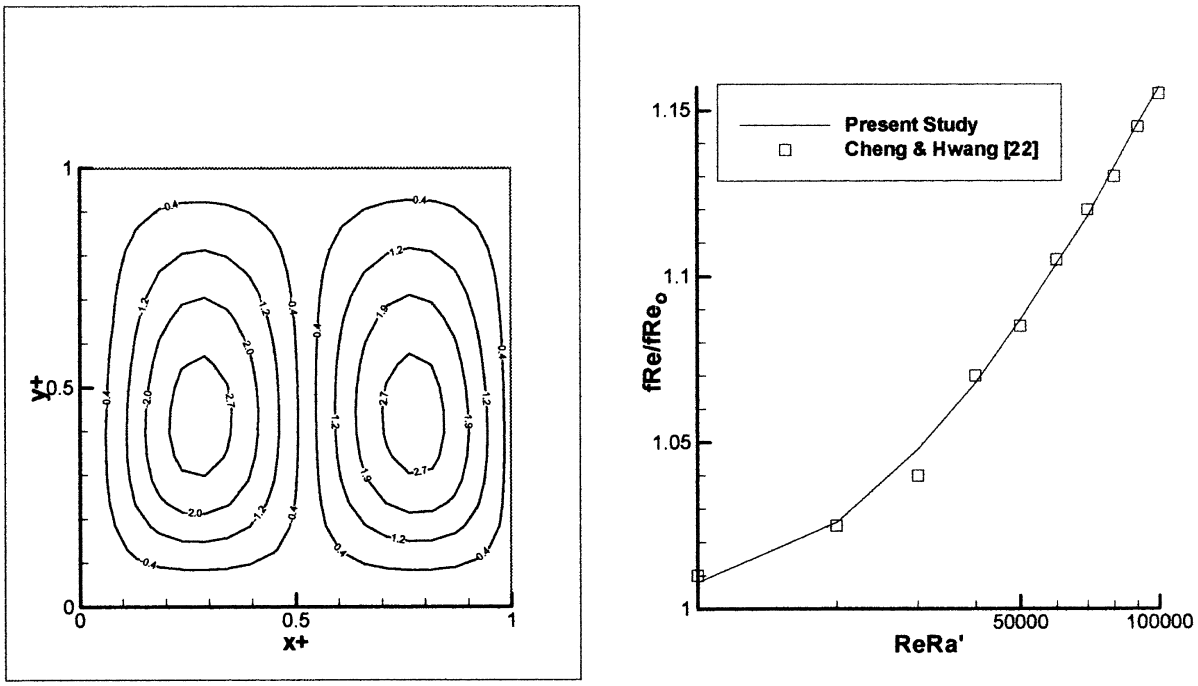

Fig. 2. Straight channel mixed convection flow field ($r^+ = 1000$, $Pr = 0.73$, $\phi = 20.0$): (a) streamlines ($Gr_g = 25\,000$); (b) friction factor ratio.

trated in Fig. 3, where $\overline{Nu}$ is presented as a function of the wall conduction parameter, ϕ. (The mixed convection data presented in Fig. 3 is discussed below in Section 4.1.5.) The forced convection solution is represented by the curve $Gr_g = 0$. To the authors' knowledge these results have not been previously presented. The asymptotic solutions for the simplified boundary conditions of uniform peripheral wall temperature and uniform peripheral heat flux at a given cross-section were calculated by assigning ϕ values of 20.0 and 0.01, respectively. The calculated results for the $H1$ and $H2$ boundary conditions are $\overline{Nu} = 3.613$ and 3.097, respectively. These solutions are in excellent agreement with data available in the literature (see, for example, Shah and London [26], who report the values 3.608 and 3.091). If we define a new parameter, ϕ_{eff}, termed the effective wall conduction parameter, as that value of ϕ at which the value of $\overline{Nu}$ is equal to 99% of the value corresponding to $\phi = \infty$ (i.e., the constant wall temperature asymptotic solution), the solution for straight channel forced convection indicates that $\phi_{\text{eff}} = 1.75$.

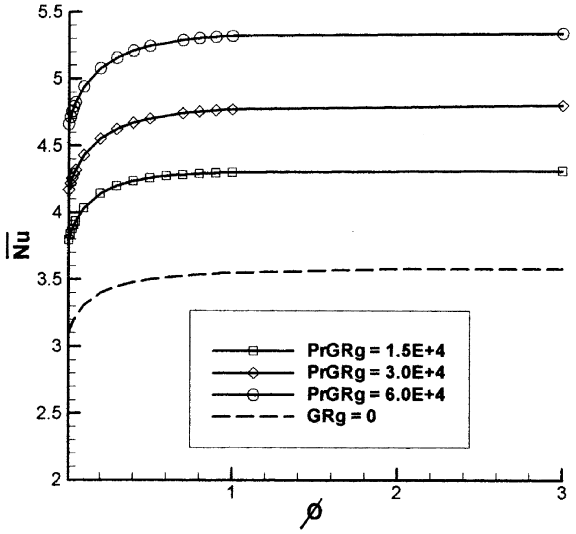

Fig. 3. Straight channel conjugated forced and mixed convection ($r^+ = 1000$, $Gr_c = 0$).

4.1.4. Mixed convection heat transfer—H1 *boundary condition* ($\text{Gr}_g \neq 0$)

The ability of the present numerical procedure to accurately model mixed convection heat transfer in a straight channel was ascertained by comparing the numerical results for $\overline{Nu}$ with those presented by Cheng and Hwang [22] for the following conditions:

$Pr = 7.20, \quad 250 \leqslant Gr_g \leqslant 2500$

$Pr = 0.73, \quad 2500 \leqslant Gr_g \leqslant 25\,000.$

The numerical results were obtained for $\phi = 20$ in order

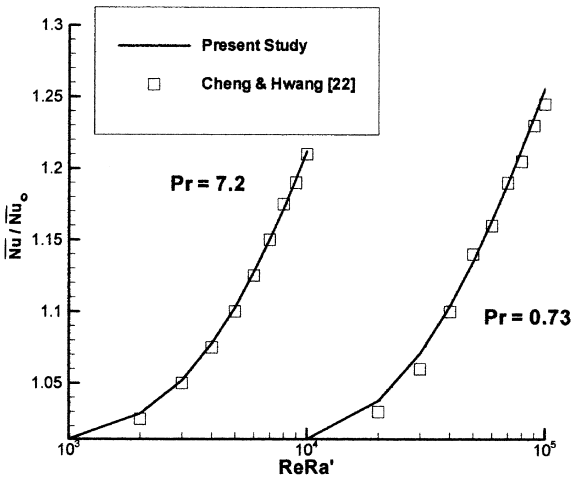

Fig. 4. Straight channel mixed convection—$H1$ boundary condition ($r^+ = 1000$, $\phi = 20.0$).

to match the constant wall temperature boundary condition of the earlier study. A plot of $\overline{Nu}/\overline{Nu}_0$ (once again, the subscript denotes the forced convection solution, $\overline{Nu}_0 = 3.613$), as a function of $Re\,Ra'$ is presented in Fig. 4. The numerical results are once again found to be in excellent agreement with the previously published data, and indicate that increased buoyancy enhances the overall straight channel heat transfer rate. It is clear that the buoyancy-induced secondary flow pattern present in the mixed convection system serves to promote heat transfer between the channel wall and fluid. In addition, it is interesting to note the strong influence of Pr on overall duct heat transfer rates, with $\overline{Nu}$ increasing quite dramatically as Pr is increased for fixed values of $Re\,Ra'$.

4.1.5. Conjugated mixed convection heat transfer ($\mathrm{Gr}_g \neq 0$)

The effect of gravitational buoyancy on straight channel conjugated heat transfer is illustrated in Fig. 3. Here, curves of $\overline{Nu}$ vs. ϕ are presented for three values of the parameter $Pr\,Gr_g$, which is the functional relationship suggested by a scale analysis performed on the governing equations (see Gyves [27]). Here we note the significant impact of buoyancy on overall heat transfer rates over the entire range of values for the wall conduction parameter, with increased buoyancy resulting in enhanced heat transfer rates for both the constant wall temperature boundary condition (as had been demonstrated earlier by Cheng and Hwang [22]) and the constant wall flux boundary condition (i.e., $\phi = 0$). As noted earlier, the buoyancy forces lead to the development of a secondary flow field consisting of two counter rotating vortices which are symmetric about the vertical centerline of the channel. The data presented in Fig. 3 indicate that this enhanced flow pattern has a significant impact on overall channel heat transfer performance. In addition, we note that the value of the mixed convection ϕ_{eff} is reduced to $0.6 \leqslant \phi_{\mathrm{eff}} \leqslant 0.8$ for the range of values of Pr and Gr_g considered. This represents a 55–65% decrease in the value of ϕ_{eff} below the forced convection value of 1.75.

4.2. Curved square channels

4.2.1. Forced convection flow field ($\mathrm{Gr}_g = \mathrm{Gr}_c = 0$)

Curved channel flows are characterized by the development of a secondary cross-stream flow pattern consisting of two counter-rotating vortices at lower values of De and four vortices at higher values of De. Figures 5(a)–(d) illustrate the development and intensification of this secondary flow field at increasing values of De. The present results indicate a transition to a four vortex flow pattern at $De = 151.1$, which is in close agreement with the results presented by Joseph et al. [28], who noted a transition at $De = 151.8$, as well as those of Ghia and Sokhey [7], who predicted a value of $De = 143$. The solutions for the Dean Number and the friction factor ratio (i.e., the ratio of the curved channel $f\,Re$ to the straight channel $f\,Re_s$) at various values of the axial pressure gradient are presented in Table 2, and are found to be in good agreement with data published in three earlier studies.

4.2.2. Mixed convection flow field (Gr_g and $\mathrm{Gr}_c \neq 0$)

For mixed convection systems, the effects of both gravitational (Gr_g) and centrifugal (Gr_c) buoyancy on the secondary flow field are presented in Figs 6(a) and (b) for the thermal boundary condition specified by $\phi = 1.0$. As can be seen by comparing Figs 5 and 6, the configuration of counter-rotating vortices located symmetrically about the horizontal channel centerline has been replaced by non-symmetric vortices skewed at an angle with the horizontal axis. As noted by Dong and Ebadian [18], gravitational buoyancy forces tend to move the fluid in the vertical direction, whereas constant density centrifugal forces act in the horizontal direction. It is interesting to note that the marked increase in Gr_g from 7500–15 000 in the present case results in only slight changes to both the magnitude and orientation of the streamlines. This would appear to indicate that the centrifugal effects are dominant for these values of (Gr_c) and (Gr_g).

4.2.3. Conjugated forced convection heat transfer ($\mathrm{Gr}_g = \mathrm{Gr}_c = 0$)

The curved channel conjugated forced convection $\overline{Nu}$ is presented in Fig. 7 as a function of both ϕ and De. It is quite evident that the heat transfer rates for curved channels are dramatically increased over those of straight channels, irrespective of the thermal boundary condition imposed on the system. The straight channel solution

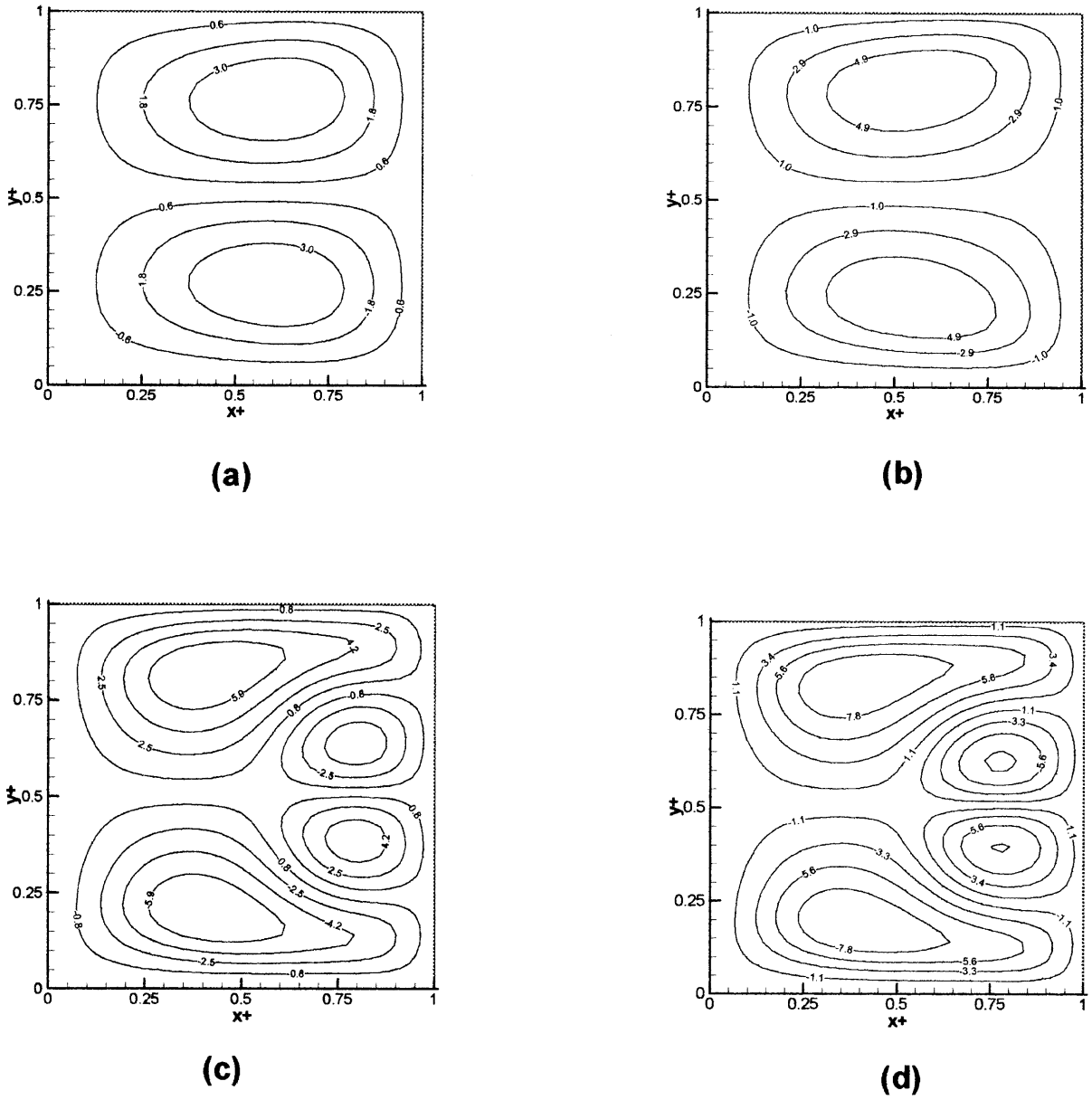

Fig. 5. Curved channel secondary flow streamlines ($r^+ = 100$, $Gr_g = Gr_c = 0$): (a) $De = 55.2$; (b) $De = 100.6$; (c) $De = 151.1$; (d) $De = 210.9$.

($r^+ = 1000$) has been included to illustrate this point. For example, at $De = 100.6$, the overall heat transfer rate is 86% higher than the straight channel heat transfer rate at $\phi = 1.0$. The results presented earlier indicate that the secondary flow field intensifies as De increases. This intensified secondary flow leads to more effective convective heat transfer between the wall and fluid and an increase in the overall heat transfer coefficient. Previous studies [10, 12] have similarly noted this marked increase in the curved square channel $\overline{Nu}$ for the $H1$ boundary condition, and the present study is in qualitative agreement with these earlier findings.

A second interesting result which the data reveal is the fact that increases in De serve to accelerate the approach to a constant wall temperature solution. That is, the value of ϕ at which one may reasonably assume a constant peripheral wall temperature boundary condition decreases with increased De. This is illustrated in Fig. 8,

Table 2
Curved channel flow field solution

			Dean number (De)				fRe/fRe_s			
dp^+/dz^+	r^+	Grid	Present study	Cheng et al. [5]	Komiyama et al. [12]	Dong and Ebadian [17]	Present study	Cheng et al. [5]	Komiyama et al. [12]	Dong and Ebadian [17]
−3950	100	30 × 30	14.0	13.9	14.0	14.1	1.01	1.01	1.00	1.00
−9000	100	30 × 30	29.7	29.5	29.8	—	1.07	1.07	1.06	—
−19 000	100	30 × 30	55.2	54.8	55.4	—	1.21	1.22	1.20	—
−39 500	100	30 × 30	100.6	100.0	101.8	99.1	1.38	1.41	1.38	1.42
−70 000	100	40 × 40	151.1	151.1	150.5	—	1.63	1.63	1.63	—
−110 000	100	40 × 40	210.9	202.6	209.5	201.4	1.83	1.91	1.91	1.92

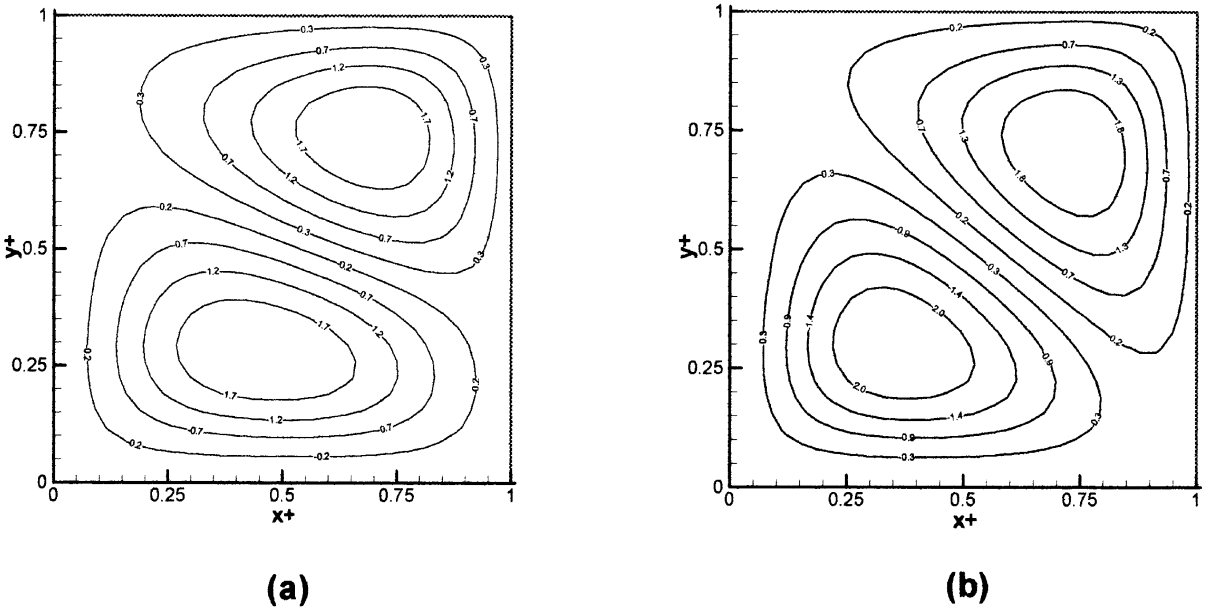

Fig. 6. Curved channel mixed convection streamlines ($r^+ = 100$, $Pr = 1$, $\phi = 1$): (a) $Gr_c = 17\,000$, $Gr_g = 7500$, $De = 65.8$; (b) $Gr_c = 17\,000$, $Gr_g = 15\,000$, $De = 65.2$.

where ϕ_{eff} is plotted against De. This curve demonstrates that for $De > 30$, the value of $\overline{Nu}$ in a curved square channel is very closely approximated by the asymptotic $H1$ solution for $\phi \geqslant 0.3$. From a practical engineering standpoint, then, curved channels need not be constructed of expensive materials with high thermal conductivities. Materials with a k_w which yields a value of $\phi = 0.3$ will provide the maximum heat transfer. From an analytical standpoint, this result provides guidance as to the point at which one must consider peripheral wall conduction a factor in the analysis. Straight square channels, it should be noted, do not benefit from any secondary flow (i.e., in the absence of gravitational buoyancy forces), and as noted earlier, the value of ϕ at which the constant wall temperature $\overline{Nu}$ can be approximated is 1.75, nearly six times the curved channel result. The benefit of improved heat transfer in curved channels must of course be weighed against the additional pump horsepower requirements resulting from the increased wall friction present in curved channel flows.

4.2.4. Mixed convection heat transfer—H1 *boundary condition* ($Gr_g \neq 0, Gr_c = 0$)

As noted earlier, all prior studies of curved channel mixed convection have included in their analysis the effect of gravitational buoyancy alone. The present study models this simplified system well, as demonstrated in Fig. 9.Here, the solution for $\overline{Nu}/\overline{Nu}_0$ (here, $\overline{Nu}_0$ represents the

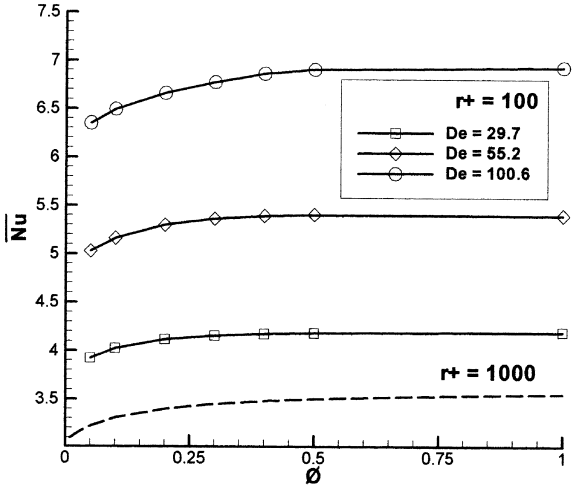

Fig. 7. Curved channel conjugated forced convection ($r^+ = 100$, $Gr_g = Gr_c = 0$).

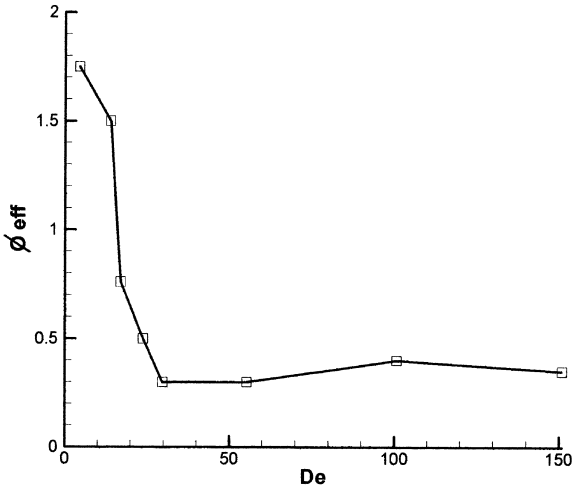

Fig. 8. Curved channel effective wall conduction parameter variation with De ($r^+ = 100$, $Gr_g = Gr_c = 0$).

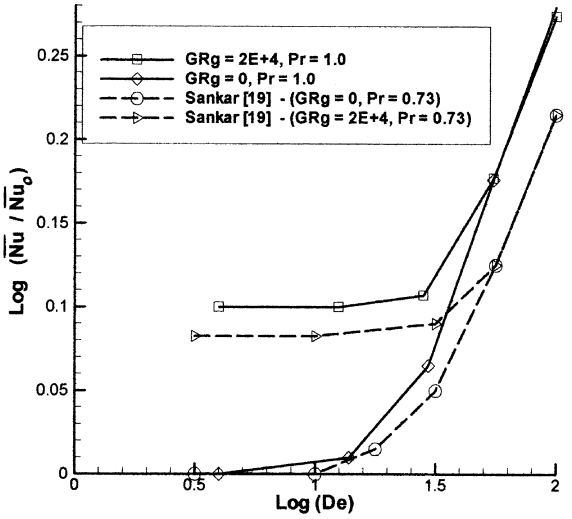

Fig. 9. Curved channel mixed convection—$H1$ boundary condition ($Gr_g \neq 0$, $Gr_c = 0$, $\phi \to \infty$).

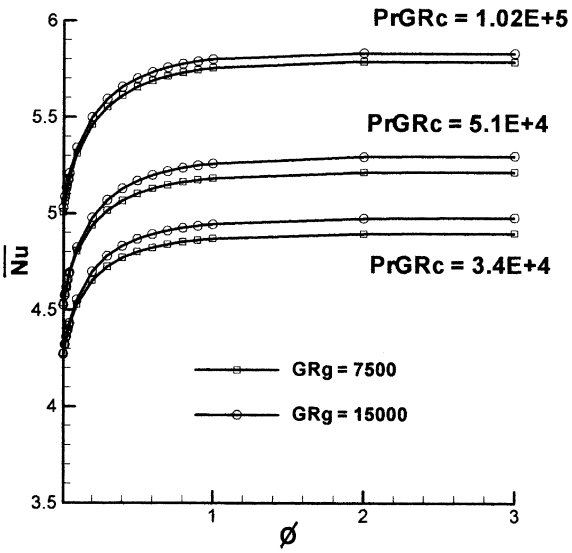

Fig. 10. Curved channel conjugated mixed convection ($r^+ = 100$, $Gr_g = 7500$ and 15 000).

straight channel forced convection value) as a function of De and Gr_g for $Pr = 1$ and $\phi \to \infty$ is compared to data presented by Sankar et al. [19] for the constant peripheral wall temperature boundary condition ($H1$) and $Pr = 0.73$. In both cases, the solution approaches the forced convection asymptote (i.e., $Gr_g = 0$) at large values of De, signifying the dominance of centrifugal forces in this region.

4.2.5. Conjugated mixed convection heat transfer (Gr_g *and* $Gr_c \neq 0$)

The numerical solution to curved channel conjugated mixed convection is illustrated in Fig. 10, with $\overline{Nu}$ presented as a function of ϕ for three values of the parameter $Pr\,Gr_c$, a functional relationship predicted by a scale analysis performed on the governing equations (Gyves [27]). The gravitational Grashof number, Gr_g, is the fourth parameter in these plots. The results presented in Fig. 10 confirm the earlier conclusion the Gr_g is a very weak parameter in curved channel mixed convection when the effects of Gr_c are also considered. Increasing Gr_g from a value of 7500–15 000 has little effect on the overall heat transfer rate over the entire range of values

of the wall conduction parameter. Clearly, centrifugal effects are dominant in curved channel flow, and this result is not unexpected. Figure 6(a) and (b) illustrates that marked increases in Gr_g do not significantly alter the secondary flow field in a curved channel with $Gr_c = 17\,000$. That is, neither the secondary flow field intensity nor the orientation of the streamlines were found to be significantly altered even when the value of Gr_g was increased from 7500–15 000.

One of the more interesting findings of the present study is the indication that, for approximately equal values of De, the curved channel mixed convection $\overline{Nu}$ values are significantly lower than those for curved channel forced convection systems for all values of the wall conduction parameter ϕ. Here it should be made clear that we are only including the effect of the centrifugal Grashof number (Gr_c) on overall heat transfer; it has already been demonstrated that the influence of Gr_g is minimal in curved channels when the effects of Gr_c are also considered. This reduction in $\overline{Nu}$ is illustrated in Fig. 11, where the forced convection value for $De = 100.6$ previously presented in Fig. 7 and the mixed convection $\overline{Nu}$ for $Pr = 1$ and $Gr_c = 34\,000$ (corresponding to $De = 94.0$), are compared. This sharp reduction in $\overline{Nu}$ can be directly attributed to the fact that despite their nearly identical values of De, the strength of the secondary flow field is dramatically reduced when one includes the centrifugal effect of variable fluid density. This can be seen by comparing the strength of the mixed convection secondary flow streamlines ($De = 94$) in Fig. 12 with those of the constant density fluid ($De = 100.6$) in Fig. 5(b). A similar reduction in both the secondary flow field intensity and $\overline{Nu}$ was presented by Goering et al. [20] in their examination of gravitational buoyancy in curved tubes, but only for the $H2$ boundary condition.

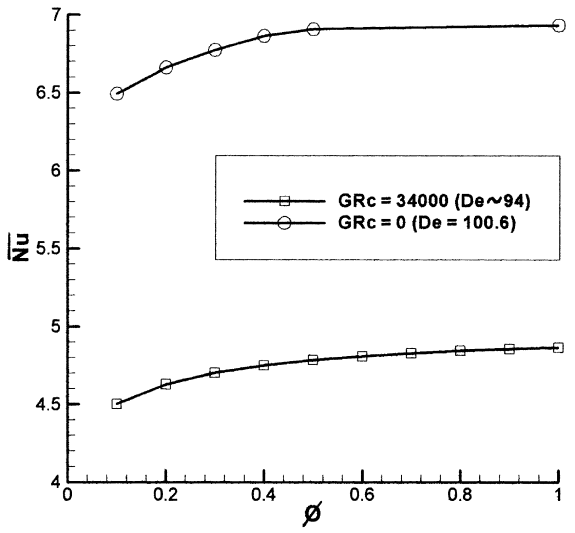

Fig. 11. Effect of centrifugal buoyancy on curved channel conjugated heat transfer ($r^+ = 100$, $Pr = 1$, $Gr_g = 0$).

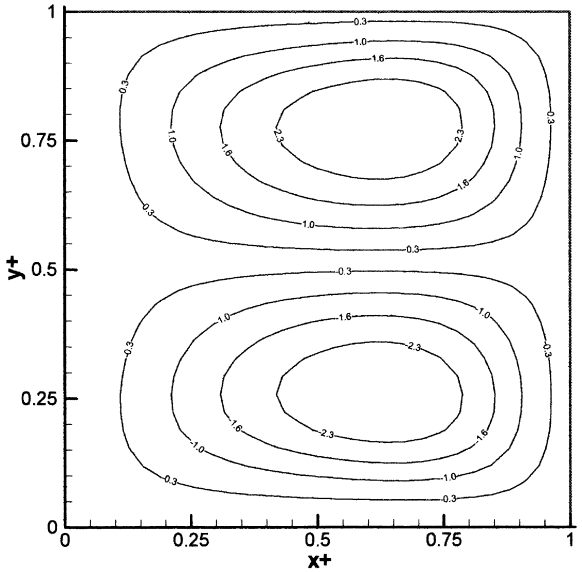

Fig. 12. Curved channel mixed convection streamline—$De = 94$ ($r^+ = 100$, $Pr = 1$, $\phi = 1$, $Gr_g = 0$, $Gr_c = 34\,000$).

Figure 13 provides additional insight into the reasons behind this reduction in the value of $\overline{Nu}$ in the mixed convection system. The local Nusselt number is defined as

$$Nu_l = \frac{1}{T_w^+ - T_b^+}\left(\frac{dT^+}{dn^+}\right)$$

and is, therefore, directly proportional to the local temperature gradient at the wall–fluid interface, dT^+/dn^+. Examination of these two figures indicates that the right wall Nu_l values for the two systems are nearly identical over the middle region of the right (i.e., outer) wall. However, in both the upper and lower regions of the right wall the temperature gradients in the forced convection system are larger than those of the mixed convection system, which is an indication that Nu_l in these areas will be larger for $Gr_c = 0$. A similar review of the left wall indicates that the forced convection Nu_l is once again higher near the top and bottom of the wall, while the mixed convection Nu_l is greater in the central region of the left wall. The local temperature gradients along the top and bottom walls indicate that the forced convection Nu_l is significantly larger along both walls. Figure 14 illustrates this comparison of the variation of Nu_l on all four walls of the curved channel for $Gr_c = 0$ and $Gr_c = 34\,000$. The distance along the duct perimeter is measured in a counter-clockwise fashion, with the bottom left corner as the starting point. The data presented in Fig. 14 is in qualitative agreement with that presented

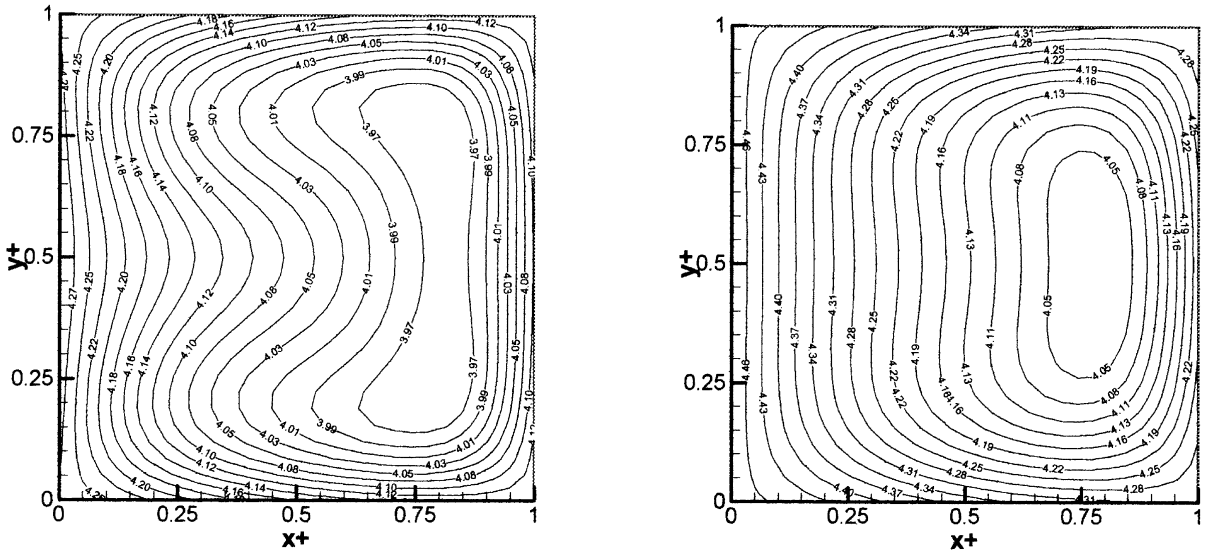

Fig. 13. Curved channel temperature contours: (a) forced convection system at $De = 100.6$ ($r^+ = 100$, $Gr_g = Gr_c = 0$, $Pr = 1$, $\phi = 1$); (b) mixed convection system at $De = 94$ ($r^+ = 100$, $Gr_g = 0$, $Gr_c = 34\,000$, $Pr = 1$, $\phi = 1$).

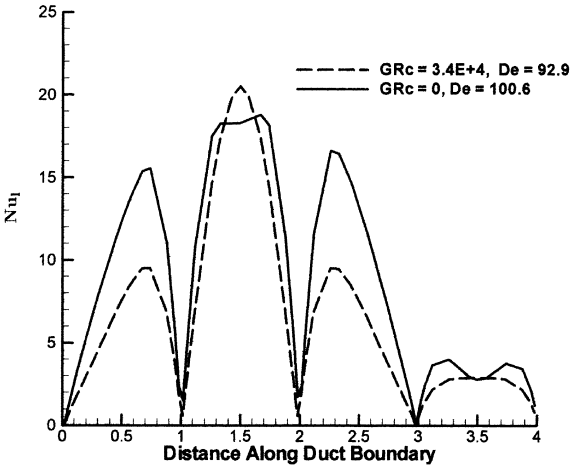

Fig. 14. Curved channel local Nusselt number profiles for forced and mixed convection systems ($r^+ = 100$, $Pr = 1$, $Gr_g = 0$, $\phi = 1$).

by Sankar et al. for $De = 32$ and $Pr = 0.73$. Thus, the decrease in $\overline{Nu}$ at $Gr_c = 34\,000$ can be explained in terms of changes in both the fluid flow field and temperature field.

5. Conclusions

The numerical solution to conjugated forced convection in straight and curved channels has been presented for the first time, and the asymptotic straight channel solutions for $\phi \to 0$ ($H2$) and $\phi \to \infty$ ($H1$) have been shown to be in strong agreement with data reported previously in the literature. The dramatic increase in the curved channel forced convection $\overline{Nu}$ over the straight channel $\overline{Nu}$ for all values of ϕ has been documented for $Gr_g = Gr_c = 0$. It has been demonstrated that one can safely assume a constant peripheral wall temperature boundary condition in forced convection systems when $De > 30$ and $\phi \geqslant 0.3$. The development of a secondary flow field in curved channels is illustrated, and the increase in $\overline{Nu}$ in curved channels can be attributed to the presence of these secondary flow vortices. Similarly, increases in gravitational buoyancy, Gr_g, have been shown to increase heat transfer in straight channels due to the introduction of a secondary flow field in the channel cross-section.

Conjugated mixed convection for fully developed flow in curved square channels has been investigated for a wide range of values of the wall conduction parameter, ϕ. Fluid density variations in both the radial and vertical directions have been examined. For the range of parameters included in the present study, changes in gravitational buoyancy (Gr_g) have been shown to have a negligible effect on $\overline{Nu}$ when the influence of centrifugal buoyancy (Gr_c) is included. For constant De, mixed convection $\overline{Nu}$ values are shown to be significantly reduced below the corresponding forced convection values due to a weakening of the secondary flow field and modifications to the fluid temperature distribution in the channel cross-section. This reduction in $\overline{Nu}$ occurs over the entire range of values of the wall conduction parameter ϕ, and not simply for the asymptotic case of $\phi \to 0$ (i.e., for the $H2$

boundary condition) as has been previously reported by Goering et al. for the case of curved tubes.

References

[1] J. Eustice, Flow of water in curved pipes, Proceedings of the Royal Society of London, Ser. A 84 (1910) 107–118.

[2] J. Eustice, Experiments on streamline motion in curved pipes, Proceedings of the Royal Society of London, Ser. A 85 (1911) 119–131.

[3] W.R. Dean, Note on the motion of fluid in a curved pipe, Philosophy Magazine 20 (1927) 208–223.

[4] W.R. Dean, The stream-line motion of fluid in a curved pipe, Philosophy Magazine 30 (1928) 673–695.

[5] K.C. Cheng, R.C. Lin, J.W. Ou, Fully developed laminar flow in curved rectangular channels, ASME Journal of Fluids Engineering 98 (1976) 41–48.

[6] S. Thangam, N. Hur, Laminar secondary flows in curved rectangular ducts, Journal of Fluid Mechanics 217 (1990) 421–440.

[7] K.N. Ghia, J.S. Sokhey, Laminar incompressible viscous flow in curved ducts of regular cross-sections, ASME Journal of Fluids Engineering 99 (1977) 640–648.

[8] Y. Mori, W. Nakayama, Study on forced convective heat transfer in curved pipes, International Journal of Heat and Mass Transfer 10 (1967) 681–695.

[9] Y. Mori, Y. Uchida, T. Ukon, Forced convective heat transfer in a curved channel with a square cross-section, International Journal of Heat and Mass Transfer 14 (1971) 1787–1805.

[10] K.C. Cheng, M. Akiyama, Laminar forced convection heat transfer in curved rectangular channels, International Journal of Heat and Mass Transfer 13 (1970) 471–490.

[11] Z. Zapryanov, C. Christov, E. Toshev, Fully developed laminar flow and heat transfer in curved tubes, International Journal of Heat and Mass Transfer 23 (1980) 873–880.

[12] Y. Komiyama, F. Mikami, K. Okui, T. Hori, Laminar forced convection heat transfer in curved channels of rectangular cross-section, Heat Transfer Japanese Research 12 (2) (1984) 68–91.

[13] G.J. Hwang, C.H. Chao, Forced laminar convection in a curved isothermal square duct, ASME Journal of Heat Transfer 113 (1991) 48–55.

[14] L.S. Yao, S.A. Berger, Flow in heated curved pipes, Journal of Fluid Mechanics 88 (1978) 339–354.

[15] J. Prusa, L.S. Yao, Numerical solution for fully developed flow in heated curved tubes, Journal of Fluid Mechanics 123 (1982) 503–522.

[16] J.B. Lee, H.A. Simon, J.C.F. Chow, Buoyancy in developed laminar curved tube flows, International Journal of Heat and Mass Transfer 28 (3) (1985) 631–640.

[17] Z.F. Dong, M.A. Ebadian, Numerical analysis of laminar flow in curved elliptic ducts, ASME Journal of Fluids Engineering 113 (1991) 555–562.

[18] Z.F. Dong, M.A. Ebadian, Effects of buoyancy on laminar flow in curved elliptic ducts, ASME Journal of Heat Transfer 114 (1992) 936–943.

[19] R. Sankar, K. Nandakumar, J.H. Masliyah, Mixed convection in heated curved square ducts, in: Proceedings of the Eighth International Heat Transfer Conference, 1986, pp. 1407–1412.

[20] D.J. Goering, J.A.C. Humphrey, R. Greif, The dual influence of curvature and buoyancy in fully developed tube flows, International Journal of Heat and Mass Transfer 40 (9) (1997) 2187–2199.

[21] E.R.G. Eckert, T.F. Irvine, Jr., Pressure drop and heat transfer in a duct with triangular cross-section, ASME Journal of Heat Transfer, 1960, pp. 125–138.

[22] K.C. Cheng, G. Hwang, Numerical solution for combined free and forced laminar convection in horizontal rectangular channels, ASME Journal of Heat Transfer, 1969, pp. 59–66.

[23] H. Miyazaki, Combined free and forced convective heat transfer and fluid flow in rotating curved rectangular tubes, ASME Journal of Heat Transfer, 1963, pp. 64–71.

[24] F. Ladeinde, K.E. Torrance, Galerkin finite element simulation of convection driven by rotation and gravitation, International Journal for Numerical Methods in Fluids 10 (1990) 47–77.

[25] S.V. Patankar, Numerical Heat Transfer and Fluid Flow, Hemisphere, 1980.

[26] R.K. Shah, A.L. London, Thermal boundary conditions and some solutions for laminar duct flow forced convection, ASME Journal of Heat Transfer 96 (1974) 159–165.

[27] T.W. Gyves, A numerical solution to conjugated mixed convection heat transfer in curved square channels, Ph.D. thesis, State University of New York at Stony Brook, Stony Brook, NY, 1997.

[28] B. Joseph, E.P. Smith, R.J. Adler, Numerical treatment of laminar flow in helically coiled tubes of square cross section, AIChE Journal 21 (5) (1975) 965–973.